ZEB1, a novel junctional adhesion molecule a regulator, impacts sensitivity of pancreatic cancer-associated fibroblasts to reovirus

Dam, N.; Harryvan, T.J.; Dang, H.; Ioannidis, G.; Schmierer, B.; Hawinkels, L.J.A.C.; Kemp, V.

Molecular Therapy
Oncology
Original Article

ZEB1, a novel junctional adhesion molecule A regulator, impacts sensitivity of pancreatic cancer-associated fibroblasts to reovirus

Nicole Dam,[1,2,4] Tom J. Harryvan,[2,4] Hao Dang,[2] Gavriil Ioannidis,[1,2] Bernhard Schmierer,[3] Lukas J.A.C. Hawinkels,[2,5] and Vera Kemp[1,5]

[1]Department of Cell & Chemical Biology, Leiden University Medical Center, Albinusdreef 2, 2333 ZA Leiden, the Netherlands; [2]Department of Gastroenterology & Hepatology, Leiden University Medical Center, Albinusdreef 2, 2333 ZA Leiden, the Netherlands; [3]CRISPR Functional Genomics, SciLifeLab and Department of Medical Biochemistry and Biophysics, Karolinska Institutet, Biomedicum Solnavägen 9, 17165 Solna, Stockholm, Sweden

Oncolytic virus (OV) therapy is a promising treatment for various tumors. However, in pancreatic ductal adenocarcinoma (PDAC), the high abundance of cancer-associated fibroblasts (CAFs) can limit OV therapy efficacy by impairing viral spread and anti-tumor immunity. We have previously shown that oncolytic reovirus infection of CAFs depends on the expression of the reovirus entry receptor junctional adhesion molecule A (JAM-A), which is not or lowly expressed in most PDAC CAFs. We propose that increasing JAM-A expression on CAFs will boost viral spread in a tumor. However, there are currently no known regulators of JAM-A expression. Therefore, we performed a genome-wide CRISPR-Cas9 knockout screen to identify novel regulators of JAM-A expression. Ablation of the top negative regulator, zinc finger E-box binding homeobox 1 (*ZEB1*), in pancreatic fibroblasts led to strong JAM-A upregulation. We show that ZEB1 directly regulates JAM-A expression by binding to the enhancer-box (E-box) regions located within the JAM-A promoter. Importantly, ZEB1 ablation increased the sensitivity of fibroblasts to reovirus infection and subsequent cell death. Our work provides a novel overview of genes regulating JAM-A expression and provides a rational approach of combining ZEB1 inhibition with reovirus therapy to target both CAFs and tumor cells in stroma-rich tumors such as PDAC.

INTRODUCTION

Oncolytic viruses (OVs) are a novel anti-cancer therapy currently tested in pre-clinical research and clinical trials for various tumor types, including pancreatic cancer.[1,2] The anti-tumor activity of OVs is attributed to a dual mechanism, relying on both the direct killing of tumor cells and indirect activation of an anti-tumor immune response through the release of immune-stimulating molecules in the tumor microenvironment (TME).[3] OVs currently tested in (pre-)clinical studies have a tropism to cancer cells either intrinsically or upon genetic manipulation.[4] However, for many tumor types, including pancreatic ductal adenocarcinoma (PDAC), the tumor-associated stroma constitutes up to 80% of the tumor mass, which could hamper the efficacy of oncolytic virotherapy.[5,6]

An important and highly abundant cell type in the TME of pancreatic cancer is the cancer-associated fibroblast (CAF). CAFs are known to influence tumor development and progression, therapy sensitivity, and anti-tumor immune responses.[7] Among many other functions, CAFs are known to induce desmoplasia by producing extracellular matrix around the tumor. Desmoplasia has been thought to influence sensitivity to OVs by, for example, hindering OV penetration and spread in the tumor and by hampering immune cell infiltration.[8,9] Furthermore, CAFs can produce cytokines and chemokines that inhibit the activity of anti-tumor immune responses.[10] Therefore, targeting CAFs with OVs, in addition to tumor cells, could be beneficial to increase overall therapy effectiveness.

While several papers have previously developed genetically modified OVs targeted to CAFs,[11–13] our group previously found that CAFs expressing the reovirus entry receptor junctional adhesion molecule A (JAM-A) can be targeted by unmodified oncolytic reovirus.[14] However, most CAFs in PDAC do not express JAM-A on their cell surface and are therefore resistant to reovirus-induced cell death. Artificial introduction of JAM-A onto JAM-A-negative fibroblasts sensitized fibroblasts to reovirus and increased reovirus infection rates in a co-culture model of tumor cells and fibroblasts.[14] While the inherent sensitivity of CAFs to several OVs has been shown before,[14–17] no studies have focused on how the sensitivity of CAFs to OVs can be increased. This could be especially relevant in those cancer types where OV-resistant CAFs dominate, like the JAM-A-negative and reovirus-resistant CAFs that characterize PDAC.[14]

Received 27 May 2025; accepted 15 October 2025;
https://doi.org/10.1016/j.omton.2025.201071.

[4]These authors contributed equally

[5]These authors contributed equally

Correspondence: Vera Kemp, Leiden University Medical Centre, Albinusdreef 2, 2333 ZA Leiden, the Netherlands.
E-mail: v.kemp@lumc.nl

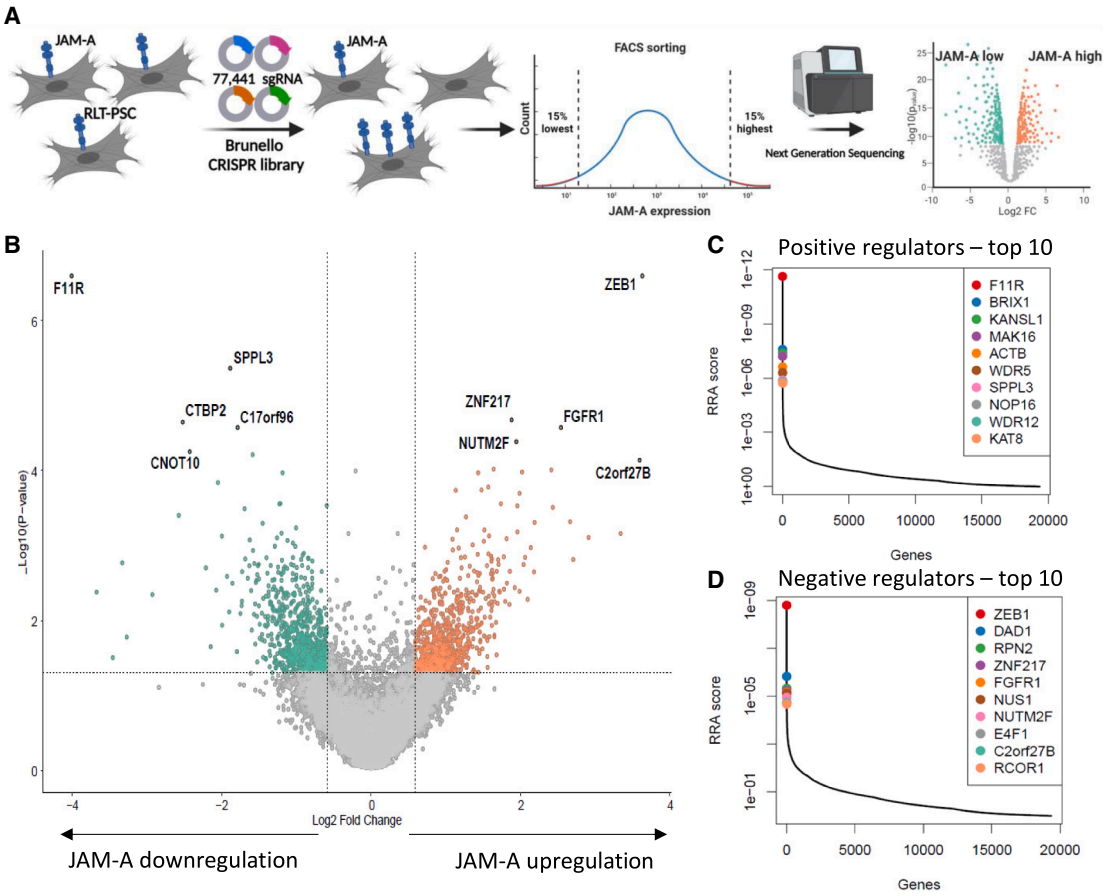

E Positive regulators

Hit	Rank (out of 19364)		P-value		Log2 fold change	
	#1	*#2*	*#1*	*#2*	*#1*	*#2*
F11R	1	1	2,56E-07	6,39E-06	-4,0108	-5,7897
BRIX1	2	9072	2,56E-07	0,47211	-3,0643	-0,54129
KANSL1	3	501	2,56E-07	0,02406	-2,049	-2,2553
MAK16	4	793	2,56E-07	0,03163	-3,1362	-1,563
ACTB	5	808	1,28E-06	0,04021	-2,2547	-2,8009
WDR5	6	1148	2,30E-06	0,05812	-1,7966	-1,4208
SPPL3	7	240	4,35E-06	0,01163	-1,8875	-4,2596
NOP16	8	151	4,86E-06	0,00725	-1,8548	-4,8777
WDR12	9	5904	5,37E-06	0,30818	-1,4034	-0,43395
KAT8	10	5	6,39E-06	9,48E-05	-2,6783	-4,2733

F Negative regulators

Hit	Rank (out of 19364)		P-value		Log2 fold change	
	#1	*#2*	*#1*	*#2*	*#1*	*#2*
ZEB1	1	146	2,56E-07	0,005526	3,6319	2,3009
DAD1	2	19	4,86E-06	0,000609	2,5058	2,0015
RPN2	3	4289	1,82E-05	0,22037	2,0543	0,49745
ZNF217	4	5340	2,12E-05	0,27377	1,8821	0,76464
FGFR1	5	4	2,68E-05	3,35E-05	2,5429	2,7591
NUS1	6	35	2,89E-05	0,001402	2,4489	2,7037
NUTM2F	7	5362	4,14E-05	0,2752	1,9448	0,72936
E4F1	8	260	7,24E-05	0,010636	1,8039	1,8493
C2orf27B	9	9491	7,29E-05	0,49925	3,5968	-2,6296
RCOR1	10	3880	8,36E-05	0,2001	1,5253	0,4869

(legend on next page)

Strategies to increase JAM-A expression would increase the sensitivity of fibroblasts, and potentially the whole tumor, to reovirus-induced cell death, and thereby increase therapy efficacy. To translate this idea into a therapeutic approach, it is imperative to understand how JAM-A expression is regulated.

Therefore, in this study, a CRISPR-Cas9 genome-wide knockout (KO) screen was performed to identify factors that regulate JAM-A expression. This screen identified zinc finger enhancer-box (E-box) binding homeobox 1 (*ZEB1*) and fibroblast growth factor receptor 1 (*FGFR1*) as strongest negative regulators of JAM-A expression. ZEB1 is a transcription factor that is well described for its role in epithelial-to-mesenchymal transcription (EMT) and regulating the expression of cell adhesion molecules like E-cadherin.[18] FGFR1 is part of the family of FGFRs, which together are responsible for a variety of biological processes, including cell growth, migration, differentiation, survival, and apoptosis.[19] Validation experiments showed that ablation of ZEB1 led to an induction of JAM-A expression, even on JAM-A-negative cell lines. Mechanistically, ZEB1 was shown to bind directly to the JAM-A promoter causing its downregulation. Reovirus replication and apoptotic cell death were increased upon partial and complete ZEB1 ablation in pancreatic fibroblasts, providing a rational approach to combine ZEB1 targeting with oncolytic reovirus to treat stroma-rich tumors like PDAC.

RESULTS

A genome-wide CRISPR-Cas9 KO screen identifies novel regulators of cell surface JAM-A expression in pancreatic fibroblasts

Given the important role of JAM-A in mediating the entry of reovirus into fibroblasts and its role in inducing virus-mediated apoptosis,[14] we performed a genome-wide CRISPR-Cas9 KO screen to identify how JAM-A expression on the cell surface of fibroblasts is regulated. RLT-PSC, a pancreatic stellate cell line with moderate JAM-A expression levels, was used to identify both positive and negative regulators of JAM-A surface expression. Stable Cas9-expressing RLT-PSCs were transduced with a genome-wide single-guide RNA (sgRNA) library,[20] and the mutagenized cell population was subsequently sorted for JAM-A^{high} and JAM-A^{low} populations (Figure 1A). The integrated guide cassettes in sorted fibroblasts were then deep sequenced to determine the relative absence or enrichment of sgRNAs, resulting in an unbiased overview of genes involved in cell surface expression of JAM-A (Figures 1A–1F; Tables S4 and S5). Among the highly significant positive regulators, in which gene KO results in reduced JAM-A surface expression, F11 receptor (*F11R*) was the top enriched hit in the JAM-A^{low} population in both replicates of the screen. *F11R* is the gene encoding JAM-A, thereby serving as a positive control of the screen and confirming its validity (Figures 1B, 1C, and 1E). Another positive regulator found enriched in the JAM-A^{low} population was *SPPL3* (Figures 1B, 1C, and 1E), a gene that was recently described to control the composition of the cell surface glycosphingolipid (GSL) repertoire by inhibiting the glycosyltransferase B3GNT5.[21]

The negative regulators of cell-surface JAM-A expression were deemed as targets of particular interest, because targeting these therapeutically could enforce stromal JAM-A expression and potentially boost reovirus activity in tumors. Two of the top hits in the JAM-A^{high} population in both replicates of the screen were *ZEB1* (rank 1/19,364 and rank 146/19,364, respectively) and *FGFR1* (rank 5/19,364 and rank 4/19,364) (Figures 1B, 1D, and 1F).

SPPL3 KO results in shielding of JAM-A on the cell surface but does not influence reovirus-mediated killing

Since SPPL3 KO was identified as a significant positive, and potentially targetable, regulator in the CRISPR-Cas9 screen, we further analyzed this hit. It has been shown that *SPPL3* KO in HAP1 cells (a haploid fibroblast-like cell line) leads to the accumulation of negatively charged neolacto-series GSLs on the cell surface.[21] This prevents human leukocyte antigen (HLA) class I (HLA-I) interactions with immune receptors, which in turn can be reversed using the clinically approved drugs miglustat and eliglustat that prevent GSL synthesis inhibition.[22] The accumulation of GSLs also leads to shielding of cell-surface HLA-I from being bound by an anti-HLA-I antibody.[21] Since JAM-A is also a cell-surface molecule, we hypothesized that shielding also occurs for JAM-A. This could potentially affect the entry of reovirus into the cell and thereby susceptibility to reovirus-induced killing. To investigate this, we performed a flow cytometry-based antibody titration assay of JAM-A on HAP1 wild-type (WT) and HAP1 *SPPL3* KO cells. At lower antibody concentrations, a clear decrease in JAM-A was observed following *SPPL3* KO, but JAM-A levels at higher antibody concentrations were almost similar between WT and *SPPL3* mutant cells, indicative of JAM-A shielding (Figures 2A and 2B). However, no apparent effect on subsequent susceptibility to reovirus-induced killing was observed between WT and *SPPL3* KO cells (Figure 2C), and therefore this target was not further pursued.

Validation of CRISPR-Cas9 screen-derived negative regulators shows that knockdown of ZEB1 results in JAM-A upregulation

To verify whether the negative regulators found in the CRISPR-Cas9 screen are valid and to determine whether partial ablation of ZEB1 and FGFR1 is sufficient to induce reovirus sensitivity on these CAFs, ZEB1 and FGFR1 knockdowns (KDs) using 2 different

Figure 1. Genome-wide CRISPR-Cas9 KO screening identifies positive and negative regulators of JAM-A expression on pancreatic fibroblasts

(A) Overview of the CRISPR-Cas9 screening approach to identify regulators of cell-surface JAM-A expression. Figure made with Biorender.com. (B) Volcano plot showing negative (green) and positive (orange) regulators of JAM-A. (C and D) The top 10 hits of positive (C) and negative (D) regulators of JAM-A cell surface expression. RRA score, robust rank aggregation score determined by MAGeCK computational tool. (E and F) Table displaying the top 10 hits displayed in (C) and (D) with corresponding rank, as determined by MAGeCK RRA score, *p* values, and log2 fold change, in both replicate 1 (left columns) and replicate 2 (right columns) of the screen.

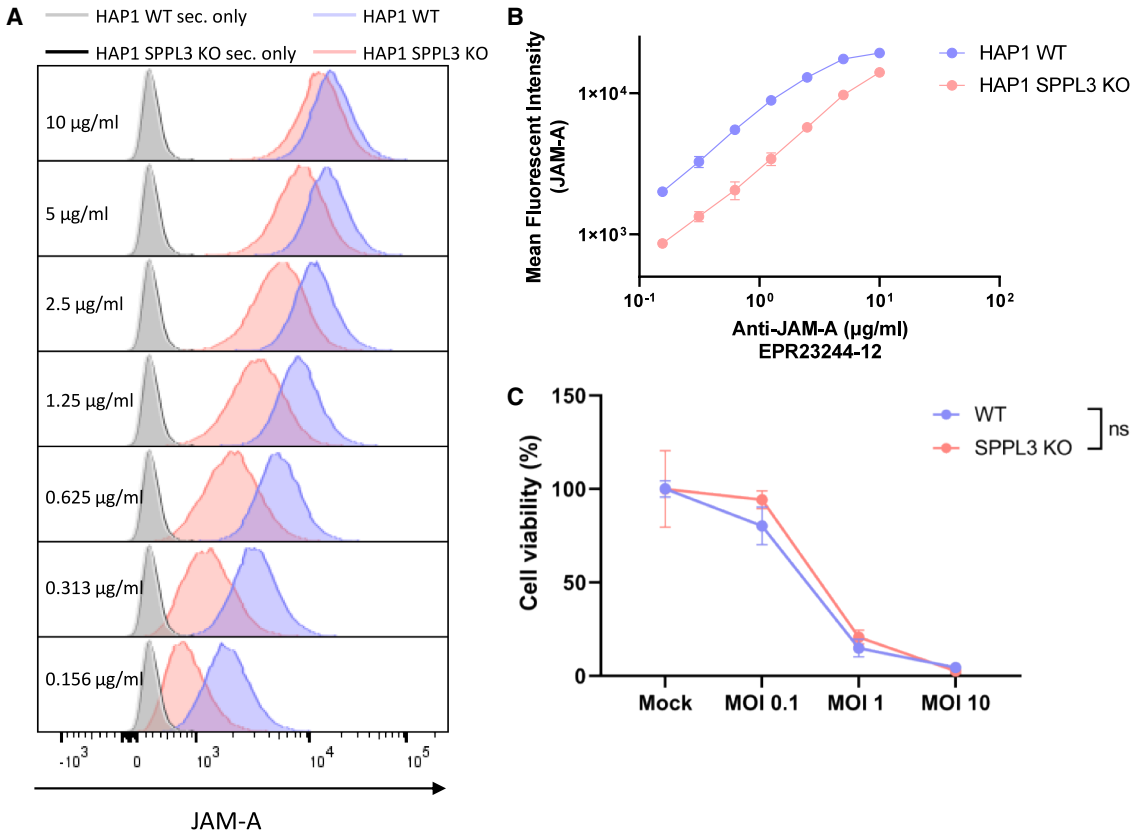

Figure 2. SPPL3 shields JAM-A from flow cytometric detection, but KO does not result in different reovirus sensitivity

(A) Flow cytometric titration of JAM-A antibody on HAP1 WT and HAP1 SPPL3 KO cells. Gray: secondary only antibody HAP1 WT, black: secondary only antibody HAP1 SPPL3 KO, blue: stained HAP1 WT, pink: stained HAP1 SPPL3 KO. (B) Mean fluorescent intensity of JAM-A at different concentrations of JAM-A antibody. Data are derived from a representative experiment and plotted as mean ± SD. (C) Cell viability (%) compared to mock of HAP1 WT and SPPL3 KO cells following 3 days reovirus infection at different MOIs, as determined by WST-1 assay. Significance was calculated using two-way ANOVA with correction for multiple testing (Šídák's test), significance is depicted at MOI 10, ns, not significant. Data are derived from a representative experiment and plotted as mean ± SD.

short hairpin RNA (shRNA) constructs were generated in the RLT-PSC stellate cell line in which the CRISPR-Cas9 screen was performed and a murine pancreatic CAF that expresses low levels of JAM-A (KPC3-CAF1). KD efficiency for both *FGFR1* and *ZEB1* was between 45% and 90% on RNA level, and ZEB1 protein decreased between 23% and 91% (Figures 3A–3F). Flow cytometric analyses of cell-surface JAM-A expression showed that FGFR1 KD did not result in upregulation of JAM-A, contrasting the results of the genome-wide CRISPR-Cas9 KO screen. However, partial shRNA-mediated ablation of ZEB1 resulted in a strong increase in JAM-A expression, in both fibroblasts with moderate (RLT-PSC) and low (KPC3-CAF1) JAM-A expression (Figures 3G and 3H), which is in line with the results of the CRISPR-Cas9 screen. Furthermore, we show that ZEB1 KD in both fibroblasts results in sensitization to reovirus-mediated cell death (Figures 3I and 3J). JAM-A upregulation and sensitization to reovirus upon ZEB1 KD, but not FGFR1, were also observed in the transformed skin fibroblast cell line NBS (Figures S1A–S1E). All in all, this shows that ZEB1 is a potent negative regulator of cell-surface JAM-A expression, and KD of ZEB1 results in JAM-A upregulation in pancreatic, but also other, fibroblasts.

Complete ZEB1 ablation in JAM-A-positive and negative human and murine fibroblast lines results in upregulation of cell-surface JAM-A expression through direct transcriptional regulation

Because of the strong effects of ZEB1 KD on JAM-A expression, we decided to further focus on ZEB1 as a potent negative regulator of JAM-A expression. We first analyzed *ZEB1* RNA expression in relation to *F11R* RNA and JAM-A protein expression in a panel of patient-derived CAFs, which have been described before.[14] We found that although there is no direct correlation between JAM-A and *ZEB1* expression, potentially due to the other negative regulators influencing JAM-A expression as well, *ZEB1* is expressed on all CAFs, providing a therapeutic window for JAM-A modulation (Figure S2). To further explore ZEB1 as a potential target, we used CRISPR-Cas9-mediated targeting of a conserved region of the *ZEB1* exon 1-intron boundary in pancreatic fibroblasts of human (RLT-PSC, hPS1) and murine (KPC3-CAF1) origin. Clonal KO

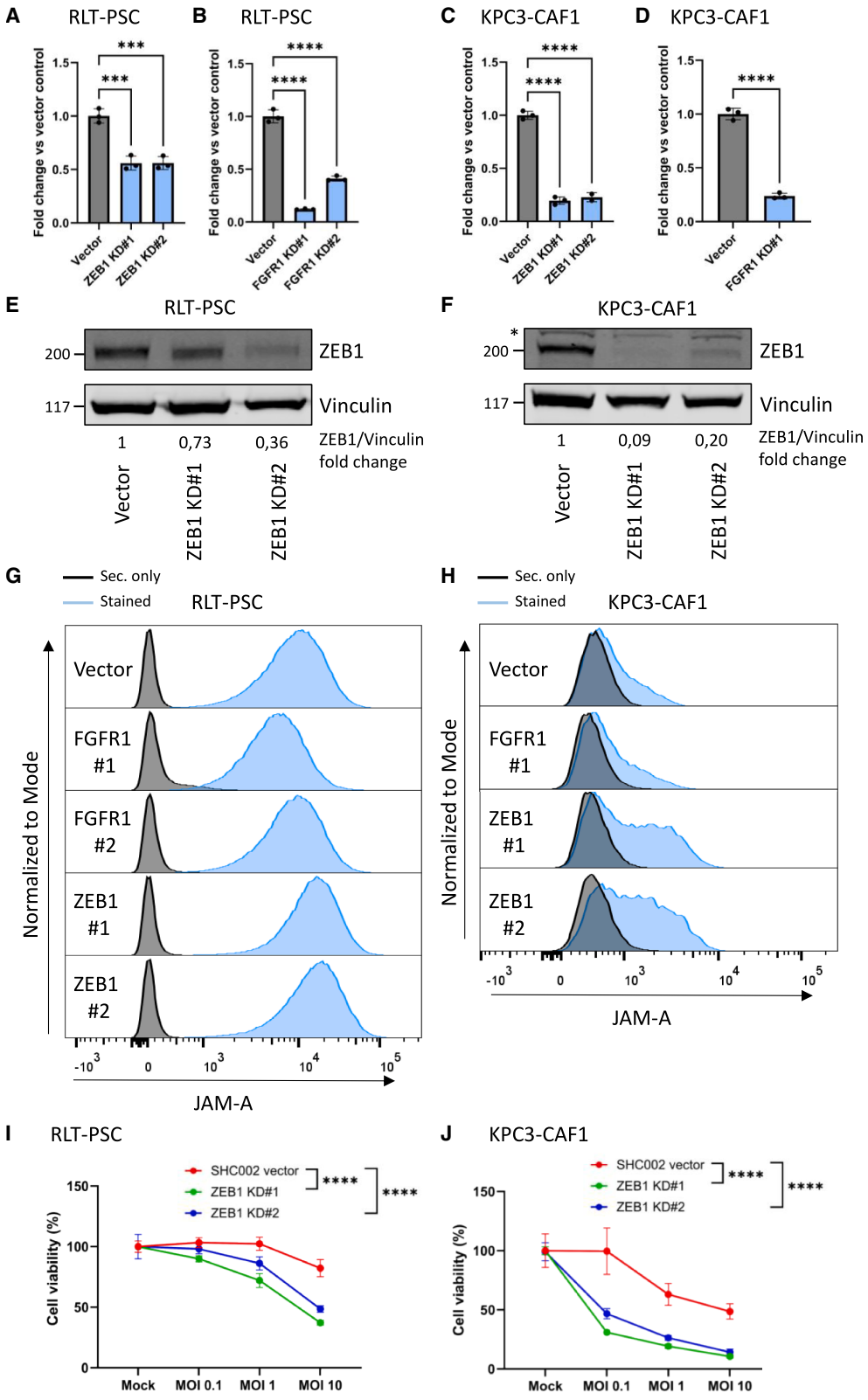

(legend on next page)

cell lines were generated by single-cell sorting and subsequently rescued by re-introducing *ZEB1* cDNA into the cells. *ZEB1* KO was validated on DNA level by PCR and Sanger sequencing of the region around the guide RNA (gRNA). Since sequencing was difficult due to high GC content of this region, PCR products were transformed in bacteria, isolated, and sequenced. This showed that indels that cause a frameshift or are large enough to disrupt the protein had occurred in all KO clones (Figures S3A–S3D). Interestingly, we could observe many different edits in the RLT-PSC KO cell lines (Figure S3B), which can be explained by the fact that RLT-PSC has a mean number of 60 chromosomes per cell[23] and thus potentially multiple *ZEB1* alleles per cell. For hPS1, 2 different indels per KO cell line could be identified, providing proof of clonality of these lines (Figure S3D). Furthermore, KO and rescue of ZEB1 protein were validated using western blot (Figures 4A–4C).

Quantitative reverse-transcription PCR (RT-qPCR) analysis revealed that ZEB1 ablation resulted in significant upregulation of *F11R* RNA levels (Figures 4D–4F). The extent of *F11R* upregulation varies within each clone, which can be attributed to the polyclonal nature of the WT cell lines.[23–25] Reintroducing *ZEB1* cDNA caused a significant downregulation of *F11R* RNA expression for all lines compared to their corresponding KO clone (Figures 4D–4F). The changes in RNA expression were also validated on protein level through flow cytometric analyses of cell-surface JAM-A expression. RLT-PSC pancreatic fibroblasts already express a moderate level of JAM-A but still showed a strong upregulation of JAM-A following ZEB1 KO (Figures 4G–4J). The most striking phenotype was observed in hPS1 (Figures 4H–4K) and the mouse pancreatic CAF KPC3-CAF1 (Figures 4I and 4L), in which ZEB1 KO transforms the cells from JAM-A negative to strongly positive. For all cell lines, reintroduction of *ZEB1* cDNA into the KOs results in a significant downregulation of JAM-A cell-surface expression (Figures 4G–4L). Since ZEB1 is an important regulator in the process of epithelial-to-mesenchymal transition, we checked whether epithelial (E-cadherin) and mesenchymal (vimentin) marker expression were changed upon ZEB1 KO. E-cadherin expression is absent in all cell lines, both WT and ZEB1 KO, while E-cadherin was detected in the epithelial control cell line BxPc3. A slight decrease in vimentin expression is observed in hPS1 ZEB1 KO cells; however, this change is not apparent following ZEB1 KO in RLT-PSC cells (Figure S4). ZEB1 is also known to regulate the expression of integrin β1,[26] a known secondary entry receptor for reovirus.[27] Therefore, we checked whether there are changes in integrin β1 following ZEB1 KO that could influence potential differences in reovirus infection. However, no differences were found in integrin β1 expression in the ZEB1 KO clones of both RLT-PSC and hPS1 fibroblasts compared to WT (Figure S5).

Since ZEB1 is known to bind directly to E-box regulatory regions within the E-cadherin (CDH1) promoter region,[28,29] we hypothesized that it also binds to E-box regions within the *F11R* (JAM-A) promoter to regulate its expression. Using a chromatin immunoprecipitation qPCR (ChIP-qPCR) assay with primers targeting different E-box sequences within the *F11R* promoter (numbered 1 to 4), we validated that ZEB1 is more enriched in binding to the *F11R* promoter when compared to isotype control antibody-bound beads. ZEB1 bound to a similar extent to the *F11R* promoter as to the *CDH1* promoter (Figure 4M). This demonstrates that ZEB1 can inhibit JAM-A expression by directly binding to the *F11R* promoter, explaining the increased levels of both JAM-A RNA and protein following ZEB1 KO.

Altogether, these data show that ZEB1 is a novel, strong regulator of JAM-A in human and murine pancreatic fibroblasts and CAFs and that ablation of this transcription factor enhances the expression of JAM-A through direct transcriptional regulation, even in fibroblasts that do not express JAM-A under basal conditions.

ZEB1 KO in pancreatic fibroblasts and CAFs increases reoviral replication and sensitizes to reovirus-induced apoptotic cell death

Having established that ZEB1 is a potent negative regulator of cell-surface JAM-A expression on pancreatic fibroblasts and CAFs, we next aimed to confirm whether ZEB1 ablation would result in increased susceptibility to reovirus infection and reovirus-mediated cell death. ZEB1 KO pancreatic fibroblasts were exposed to different reovirus concentrations, followed by assessment of cell viability, caspase 3/7 activation to determine activation of the apoptotic pathway, and assessment of reovirus protein σ3 levels in the cell as a measure for viral infection and replication. While RLT-PSC WT, due to its moderate JAM-A expression, can be killed by reovirus, ZEB1 KO

Figure 3. ZEB1 KD, but not FGFR1 KD, results in increased JAM-A expression in JAM-A-positive and negative human and murine fibroblast cell lines and sensitization to reovirus

(A–D) RT-qPCR for *ZEB1* expression in RLT-PSC (A) and KPC3-CAF1 (C) vector control and ZEB1 KD and *FGFR1* expression in RLT-PSC (B) and KPC3-CAF1 (D) vector control and FGFR1 KD. Ct values were corrected for *IPO8* and *EIF2B1* (RLT-PSC) or *Mzt2* and *Ptp4a* (KPC3-CAF1) expression and calculated as fold change vs. vector control. Significance was calculated using one-way ANOVA with correction for multiple testing (Šídák's test) or unpaired *t* test for KPC3-CAF1 FGFR1 KD, ***$p \leq 0.001$, ****$p \leq 0.0001$. Data are derived from a representative experiment and plotted as mean ± SD. (E and F) Western blot for ZEB1 (200 kDa) with vinculin (117 kDa) as loading control in RLT-PSC (E) and KPC3-CAF1 (F) vector control and ZEB1 KD. Asterisk indicates a specific band. Band intensity was determined using Image Studio Lite software and calculated as fold change versus the WT cell line. (G and H) Flow cytometric analysis of cell-surface JAM-A expression in RLT-PSC (G) and KPC3-CAF1 (H) vector control, FGFR1 KD, and ZEB1 KD. Black: secondary antibody only, blue: stained. (I and J) Cell viability (%) relative to mock following infection of RLT-PSC (I) and KPC3-CAF1 (J) vector control and FGFR1 and ZEB1 KDs with reovirus at multiple MOIs for 3 days, as measured by a WST-1 assay. Significance was calculated using two-way ANOVA with correction for multiple testing (Šídák's test), significance is depicted at MOI 10, ****$p \leq 0.0001$. Data are derived from a representative experiment and plotted as mean ± SD.

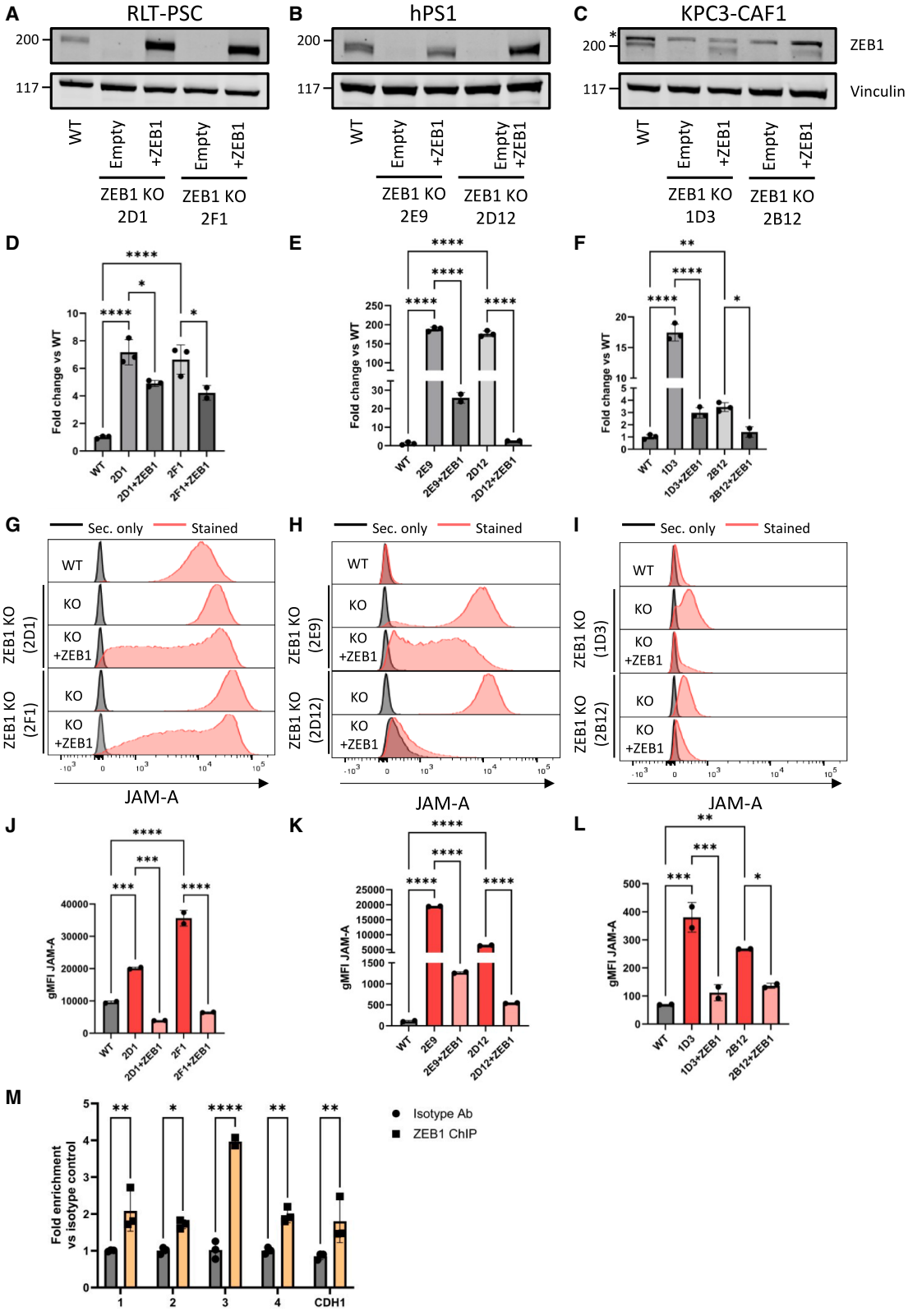

(legend on next page)

significantly increased reovirus-induced cell death at high MOI (Figure 5A). Furthermore, we show that this increased level of cell death is mediated through apoptotic cell death (Figures 5B and 5C; Video S1). In addition to increased levels of cell death, we also observed increased levels of reovirus σ3 protein in ZEB1 KO clone 2D1, indicative of increased reovirus replication (Figure 5D). Of note, while clone 2F1 did not show increased σ3 levels (Figure 5D), JAM-A expression (Figure 4G) and cell death (Figure 5A) were strongly increased. While hPS1 WT is not susceptible to reovirus, ZEB1 KO in this cell line strongly increased both reovirus replication and apoptotic cell death (Figures 5E–5H; Video S1). Similarly, ZEB1 KO in the murine CAF line KPC3-CAF1 resulted in higher levels of viral replication, reovirus-induced cell death, and caspase 3/7 activation (Figures 5I–5L; Video S1). Finally, restoring ZEB1 expression in the ZEB1 KO clones either completely or partially restored the resistance to reovirus-mediated cell death (Figures 5A, 5E, and 5I).

All in all, this shows that ZEB1 ablation in pancreatic fibroblasts, in addition to causing JAM-A upregulation, can increase their susceptibility to reovirus infection and reovirus-mediated apoptotic cell death.

DISCUSSION

In this study, we identified ZEB1 as a key factor regulating the expression of the reoviral entry receptor JAM-A, using a genome-wide CRISPR-Cas9 KO screen in fibroblasts. Clonal ZEB1 KOs and KDs in three different pancreatic fibroblast cell lines indeed showed an upregulation of JAM-A cell-surface expression and subsequent sensitization to reovirus replication and reovirus-mediated cell death. Interestingly, a partial ZEB1 KD is already sufficient to induce sensitivity to reovirus. Since a partial KD is more feasible to achieve in a patient compared to a full KO, this finding highlights the potential to clinically translate these findings. Mechanistically, we show that ZEB1 binds directly to E-box regulatory regions located within the JAM-A promoter, thereby repressing its transcription.

The field of oncolytic virotherapy has, until recently, focused on finding and developing tumor-selective viruses that leave healthy cells intact.[30] While this improves safety, it can also limit efficacy by preventing targeting of other components in the TME. In several tumor types, including PDAC, a large part of the tumor stroma consists of CAFs,[5] which can form a barrier to the efficacy of OV therapy. Therefore, strategies to also target the PDAC stroma, such as presented here, hold great potential to improve the therapeutic efficacy of the viruses.

Several groups have focused on generating genetically modified OVs directed against CAFs.[11–13] Intriguingly, we previously found that reovirus inherently has the capacity to target stromal components as long as they express the reovirus entry receptor JAM-A.[14] Reovirus is particularly interesting for extending its tropism because it is non-pathogenic and causes a self-limiting infection in humans,[31] in contrast to other OVs.[32] We observed that reovirus-sensitive CAFs boosted overall viral spread in a multicellular tumor model compared to reovirus-resistant CAFs.[14] Importantly, the majority of pancreatic CAFs express very low levels of JAM-A. Two approaches to boost the CAF tropism of reovirus could be (1) modulating the viral vector to allow JAM-A independent entry[33] and (2) modulating the stroma to allow WT reoviral infection. Since JAM-A is crucial for the induction of reovirus-mediated apoptosis,[14] JAM-A-independent entry could potentially interfere with the cytolytic capacity of these viruses. Furthermore, we found that there is also a strong correlation between the JAM-A expression on fibroblasts and cell death induced by our JAM-A-independent reovirus Jin-3, showing that in the presence of JAM-A, Jin-3 will still use this receptor to enter cells more efficiently.[14] Therefore, modulating the stroma to increase reovirus infection of CAFs in a JAM-A-dependent manner seems an attractive alternative. In order to increase the overall efficacy of reovirus therapy in pancreatic tumors, we propose to increase CAF targeting through upregulating JAM-A on their cell surface. While inherent targeting of CAFs by OVs has been shown,[14–17] we are the first to increase sensitivity of CAFs to oncolytic reovirus, through upregulation of JAM-A.

Although the initial screen also identified *FGFR1* as a potent negative regulator of JAM-A expression, FGFR1 KD in both the RLT-PSC fibroblast cell line in which the screen was performed, and the murine CAF line KPC3-CAF1, did not result in JAM-A upregulation. Since the other hit, *ZEB1*, did show a strong JAM-A upregulation, this factor was further pursued. ZEB1 has been described as one of the main transcription factors regulating EMT. Furthermore, it regulates the expression of various cell-adhesion molecules, including E-cadherin.[18] Since JAM-A is also a cell-adhesion molecule like

Figure 4. ZEB1 KO in human and murine pancreatic fibroblasts results in increased JAM-A RNA and protein through direct transcriptional regulation

(A–C) Western blot of clonal ZEB1 KO and ZEB1 rescues (200 kDa) in RLT-PSC (A), hPS1 (B), and KPC3-CAF1 (C) fibroblasts with vinculin (117 kDa) as loading control. Asterisk indicates a specific band. (D–F) RT-qPCR analysis of *F11R* expression in ZEB1 KO and rescue cell lines RLT-PSC (D), hPS1 (E), and KPC3-CAF1 (F). Ct values were corrected for *IPO8* and *EIF2B1* (RLT-PSC and hPS1) or *MZT2* and *PTP4A2* (KPC3-CAF1) expression and calculated as fold change vs. WT. $^{*}p \leq 0.05$, $^{**}p \leq 0.01$, $^{****}p \leq 0.0001$ as determined by one-way ANOVA with correction for multiple testing (Šídák's test) Data are derived from a representative experiment and plotted as mean ± SD. (G–I) Flow cytometric analyses of cell-surface JAM-A expression of ZEB1 KO clones and rescues in RLT-PSC (G), hPS1 (H), and KPC3-CAF1 (I). Black: secondary only antibody, red: stained. (J–L) Geometric mean fluorescent intensity (gMFI) of JAM-A expression of the different cell lines as depicted in (G), (H), and (I). $^{*}p \leq 0.05$, $^{**}p \leq 0.01$, $^{***}p \leq 0.001$, $^{****}p \leq 0.0001$ as determined by one-way ANOVA with correction for multiple testing (Šídák's test). Data are derived from a representative experiment and plotted as mean ± SD. (M) Chromatin immunoprecipitation qPCR (ChIP-qPCR) assay to identify DNA binding regions of ZEB1. 1–4: different E-box binding regions within the F11R promoter, CDH1: E-box binding region within the E-cadherin promoter. $^{*}p \leq 0.05$, $^{**}p \leq 0.01$, $^{****}p \leq 0.0001$ as determined by two-way ANOVA with correction for multiple testing (Šídák's test). Data are derived from a representative experiment and plotted as mean ± SD.

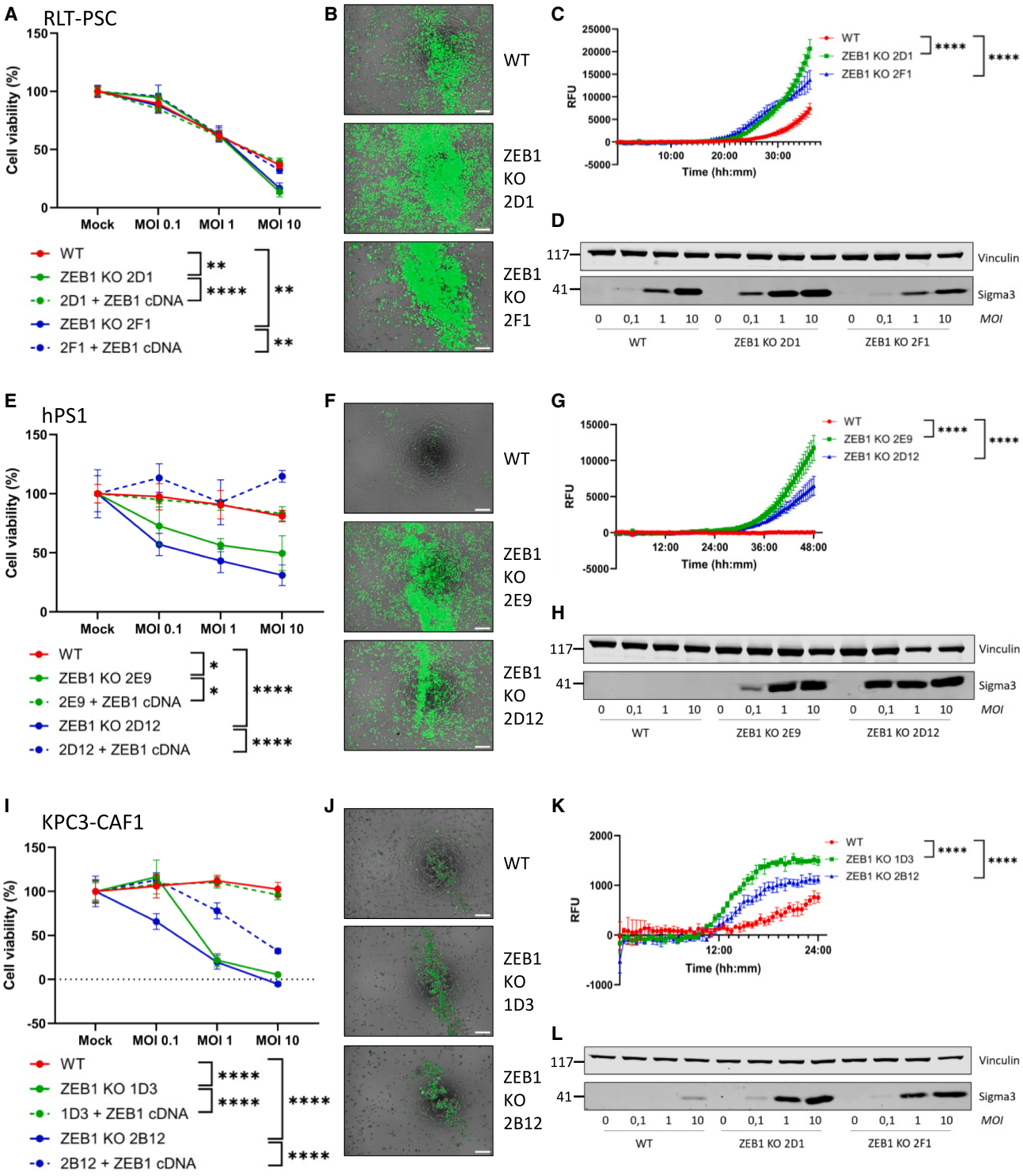

Figure 5. ZEB1 KO in human and murine fibroblasts results in increased susceptibility to reovirus infection and reovirus-mediated apoptotic cell death

(A, E, and I) Cell viability (%) relative to mock following infection with reovirus at multiple MOIs, as measured by a WST-1 assay. RLT-PSC (A) were infected for 4 days, hPS1 (E) for 6 days, and KPC3-CAF1 (I) for 3 days. Significance was calculated using two-way ANOVA with correction for multiple testing (Šídák's test), significance is depicted at MOI 10, $^{*}p \leq 0.05$, $^{**}p \leq 0.01$, $^{****}p \leq 0.0001$. Data are derived from a representative experiment and plotted as mean ± SD. (B, F, and J) Overlay of phase-contrast and GFP images of CellEvent Caspase 3/7 assay of RLT-PSC (B), hPS1 (F), and KPC3-CAF1 (J) WT and ZEB1 KO cells. Cells were infected with R124 MOI 10 for 36, 48, and 24 h,

(legend continued on next page)

E-cadherin, it is interesting to find that expression of both proteins is regulated by ZEB1.[19] ZEB1 suppresses E-cadherin expression by binding to E-box regulatory motifs,[28,29] and we show here that ZEB1 also binds to several E-box regulatory motifs present in the promoter of the *F11R* gene, which encodes JAM-A. While this was experimentally validated in CAFs, ZEB1 can also bind to E-box motifs in the *F11R* promoter in different cell types, as long as they express ZEB1. This shows that our findings can be translated to other cell types that express ZEB1. Although ZEB1 is highly expressed in CAFs, tumor cells that undergo EMT, a common phenomenon during tumor progression, also upregulate ZEB1.[34,35] Loss of JAM-A in tumor cells during tumor progression has been observed in patients with PDAC and is associated with adverse clinical outcome.[36] Therefore, targeting of ZEB1 could potentially also restore JAM-A expression in these mesenchymal tumor cells, sensitize them to reovirus infection, and perhaps even revert EMT. While we show that ZEB1 KO in fibroblasts does not lead to significant changes in markers of EMT, others have shown that silencing ZEB1 in tumor cells can actually revert EMT, thereby reducing tumor aggressiveness.[37]

Interestingly, a recent paper also showed important roles of ZEB1 expression in CAF polarization, promoting myofibroblastic features and restricting immune activation. ZEB1 ablation in fibroblasts of mice bearing colorectal cancer impaired the barrier function of CAFs by decreasing collagen deposition. Furthermore, it increased cytokine production by CAFs, which led to lymphocyte attraction and effective anti-tumor immune responses.[38] Similar effects were observed in a murine model of breast cancer.[39] Both effects of ZEB1 ablation in fibroblasts, decreased barrier function and increased immune activation, point to a strong synergistic anti-tumor effect when combined with reovirus therapy, increasing both viral spread and enhancing reovirus-induced anti-tumor immunity. Additionally, ZEB1 has also been shown to have pro-tumorigenic effects in other components of the TME by mediating interleukin (IL)-2 suppression in tumor-specific T cells. Therefore, inhibiting ZEB1 activity will restore IL-2 expression in T cells, resulting in increased T cell proliferation and homeostasis.[40] Thus, in addition to sensitizing CAFs to reovirus, there are multiple rationales why targeting ZEB1 in the PDAC TME, together with reovirus treatment, is an attractive treatment option.

In addition to finding ZEB1 as a potent JAM-A regulator, the CRISPR-Cas9 screen identified many more novel JAM-A regulators, which could be followed up on. While we focus here on the effect of JAM-A upregulation on reovirus-mediated targeting of CAFs, JAM-A is expressed in a variety of tissues and cell types and has a multitude of functions. For example, it can regulate epithelial and endothelial barrier function, hemostasis, angiogenesis, and development.[41] Furthermore, it has been implicated in diseases other than cancer, such as atherosclerosis and systemic sclerosis.[42,43] Therefore, our findings are also relevant for many other fields of research, in addition to cancer and specifically OV research.

In conclusion, using unbiased CRISPR-Cas9 genome-wide KO screening, we identified previously unknown regulators of cell-surface JAM-A expression on CAFs and validated ZEB1 as a potent negative regulator. This will allow the design of rational combination treatments targeting ZEB1 to convert naturally resistant PDAC CAFs to a reovirus-susceptible stroma, which will allow concurrent targeting of both tumor cells and CAFs.

MATERIALS AND METHODS

Cell culture

KPC3-CAF1,[25] the pancreatic stellate lines hPS1 (kindly provided by H. Kocher, University of London, London, England)[24] and RLT-PSC,[23] and BxPc3 were maintained in Dulbecco's modified Eagle's medium (DMEM)/F12 (Thermo Fisher Scientific, Leiden, the Netherlands), supplemented with 8% fetal calf serum (FCS), 100 IU/mL penicillin, and 100 μg/mL streptomycin (all Thermo Fisher Scientific). HAP1 WT and SPPL3 KO cells (kind gift of Dr. M. Jongsma, Dept. Cell & Chemical Biology, LUMC, the Netherlands)[21] were cultured in DMEM supplemented with 8% FCS, 100 IU/mL penicillin, and 100 μg/mL streptomycin (all Thermo Fisher Scientific). All cells were cultured at 37°C and 5% CO_2 and routinely confirmed to be negative for mycoplasma contamination. Genetic modification of cell lines is described in the section lentiviral transductions and transgenic cell lines.

OVs

The WT type 3 Dearing (T3D) reovirus strain R124 was isolated by plaque purification from a heterogenous T3D stock obtained from ATCC (VR-824) and propagated and purified as described previously.[33] Infections of cells with R124 were performed in the standard culture medium with 2% FCS.

Flow cytometry and fluorescence-assorted cell sorting

For cell surface staining, cells were harvested and washed twice with fluorescence-assorted cell sorting (FACS) buffer, consisting of PBS/0.5% bovine serum albumin (BSA, Sigma-Aldrich, Amsterdam, the Netherlands) and 0.05% sodium azide (Pharmacy LUMC, Leiden, the Netherlands). Human fibroblasts were incubated with rabbit anti-human JAM-A (EPR23244-12, Abcam, Cambridge, UK) at 4°C for 45 min. Subsequently, cells were washed twice with FACS buffer and incubated with goat anti-rabbit-PE (Jackson ImmunoResearch Europe Ltd, United Kingdom) at 4°C for 45 min. For murine samples, cells were incubated with a directly AF488-conjugated rat

respectively. Scale bars: 200 μM. (C, G, and K) Quantification of CellEvent Caspase 3/7 fluorescent signal over time, during infection with reovirus R124 MOI 10 for 36 (RLT-PSC, C), 48 (hPS1, G), or 24 h (KPC3-CAF1, K). Significance was calculated using two-way ANOVA with correction for multiple testing (Šídák's test), $^{****}p \leq 0.0001$. Data are derived from a representative experiment and plotted as mean ± SD. (D, H, and L) Western blot for reovirus Sigma3 expression (41 kDa) and vinculin (117 kDa) as loading control in WT and ZEB1 KO cells following reovirus infection at different MOIs. RLT-PSC (B) and hPS1 (E) were infected for 2 days and KPC3-CAF1 (H) for 1 day.

anti-mouse JAM-A (H202-106, Bio-Rad Laboratories, Nazareth, Belgium) at 4°C for 45 min. For integrin beta-1 (CD29) staining, human fibroblasts were incubated with a PE-conjugated mouse anti-human CD29 (MAR4, BD biosciences, Drachten, the Netherlands) at 4°C for 45 min. Samples were measured on an LSR-II flow cytometer (BD biosciences), and data were analyzed with FlowJo software, v.10.6.1 (BD Biosciences). For single-cell sorting of ZEB1 KO clones, an Aria FACS sorter (BD Biosciences) was used. For cell sorting of RLT-PSC fibroblasts in the CRISPR-Cas9 KO screen, cells were sorted using a Sony SH800 cell sorter (Sony Biotechnology Inc., San Jose, CA, USA).

Genome-wide CRISPR-Cas9 KO library screen

Generation of stable Cas9-expressing fibroblasts

RLT-PSC fibroblasts were lentivirally transduced with pLenti-Cas9-T2A-Blast-BFP (Addgene #196714) to express a codon-optimized, WT SpCas9 flanked by two nuclear localization signals linked to a blasticidin-S-deaminase—mTagBFP fusion protein via a self-cleaving peptide. Following blasticidin selection, a stable BFP+ population was isolated by repeatedly sorting for BFP expression until >90% Cas9+/BFP+ was obtained.

Guide library

The genome-wide Brunello sgRNA library[20] was synthesized as 79-bp-long oligos (CustomArray, GenScript). The oligo pool was double-stranded by PCR using ds_Ultramer and amplification with primers ds_fw and ds_rev (Table S1) to include an A-U flip in the tracrRNA,[44] 10-nucleotide-long random sequence labels, and an i7 sequencing primer-binding site.[45] The resulting PCR product (Table S1) was cloned by Gibson assembly into pLenti-Puro-AU-flip-3xBsmBI (Addgene #196709).[45] The plasmid library was input sequenced to confirm representation and packaged into lentivirus in HEK293T (ATCC) using plasmids psPAX2 (a gift from Didier Trono, Addgene #12260) and pCMV-VSV-G (a gift from Bob Weinberg, Addgene #8454). The virus-containing supernatant was concentrated with Lenti-X concentrator (Takara, Saint-Germain-en-Laye, France), aliquoted, and stored in liquid nitrogen.

Library virus titration and large-scale transduction

The functional titer of the library virus was estimated from the fraction of surviving RLT-PSC cells after transduction of target cells with different amounts of virus and puromycin selection. For the screen, Cas9-BFP-expressing target cells were transduced with the library virus in duplicate at an approximate MOI of 0.3 and a coverage of 500–1,000× (500–1,000 cells per guide) in the presence of 2 μg/mL polybrene. Transduced cells were selected with 2 μg/mL puromycin from day 2 to day 6 post transduction. A control sample worth 80 million cells per replicate was harvested at day 5 post transduction. Cell numbers per replicate were kept at $\geq$ 80 million/replicate throughout to ensure full library coverage.

At day 7 post transduction, RLT-PSC cells were stained as described earlier and two-way FACS-sorted based on the expression of JAM-A, with collection of the lowest (15%) and highest (15%) JAM-A-expressing cells. Collected cell pellets were stored at −20°C until the extraction of genomic DNA.

Genomic DNA, library preparation, and next-generation sequencing

Genomic DNA was isolated using the QIAamp DNA Blood Maxi or Mini Kit (QIAGEN, Venlo, the Netherlands), and guide and UMI sequences were amplified in a three-step PCR protocol as described,[45] using the primers given in Table S1. The amplicon was sequenced on Illumina NovaSeq6000, reading 20 cycles read 1 with custom primer CRISPRSeq (Table S1); 10 cycles index read i7 to read the UMI, and six cycles index read i5 for the sample barcode. Next-generation sequencing data were analyzed with the MaGeCK software, v.0.5.6.[46]

Lentiviral transductions and transgenic cell lines

For all lentiviral constructs, third-generation packaging vectors and HEK293T cells were used for the generation of lentiviral particles.[47] To generate ZEB1 KO fibroblast cell lines (hPS1, RLT-PSC, and KPC3-CAF1), a sgRNA, 5′-caccgCACTCACCGT TATTGCGCCG-3′ (lowercase nucleotides are compatible with the restriction site) targeting a conserved region of the *ZEB1* exon 1-intron boundary was cloned into *BsmBI*-digested plenti-CRISPRv2-hygromycin (Addgene: #98291). This design enables targeting of both murine and human *ZEB1* with the same construct. Lentiviral particles were generated, and after transduction, hygromycin-resistant fibroblasts were sorted, based on their gain of JAM-A expression (highest 5%), at single-cell density and subsequently expanded to acquire clonal lines. Cells were selected with 200 μg/mL of hygromycin B (Merck). KO verification of clones was performed via western blot and DNA sequencing.

Rescue of the ZEB1 KO was performed by reintroducing human *ZEB1*-encoding cDNA, which was amplified from a fibroblast cDNA library using primers 5′-gatcctcgagaccATGGCGGATGGCC CC-3′ (forward, *XhoI* restriction site) and 5′-gatcaccggtTTAGGCT TCATTTGTCTTTTC-3′ (reverse, *AgeI* restriction site) using the Phusion High-Fidelity PCR Kit according to manufacturer's instructions (Thermo Fisher Scientific). The resulting PCR product was gel purified using the NucleoSpin Gel and PCR Clean-up kit (Macherey-Nagel, Dueren, Germany), and 3′ A-overhangs were added by incubation with *Taq*-polymerase (DreamTaq Green PCR Master Mix [Thermo Fisher Scientific]) for 30 min at 72°C. This product was cloned into the pCR4-TOPO TA vector using the TOPO TA Cloning kit according to manufacturer's instructions (Thermo Fisher Scientific). Subsequently, this clone was fully sequenced and confirmed to be *ZEB1* transcript variant 2 (CCDS7169). Lastly, this cDNA was subcloned into pLV-CMV-puromycin[14] and termed pLV-CMV-*ZEB1*-puromycin. For hPS1, since these already contain a puromycin resistance cassette, *ZEB1* cDNA was cloned into pLV-CMV-neomycin. Clonal ZEB1 KO cells were transduced with this vector and selected and subsequently cultured with puromycin (2 μg/mL; Sigma-Aldrich) or G418 (400 μg/mL; Thermo Fisher Scientific). Finally, ZEB1 rescue was confirmed through western blot.

KD constructs were acquired from the Mission TRC shRNA library (Sigma-Aldrich), with target sequences that are shown in Table S2. Cells were selected and cultured with 2 μg/mL puromycin (Sigma-Aldrich).

RNA isolation and RT-qPCR analysis

Total RNA was isolated using the NucleoSpin RNA isolation kit (Macherey-Nagel, Düren, Germany) according to manufacturer's instructions. cDNA was synthesized using SuperScript II Reverse Transcriptase (Invitrogen, Thermo Fisher Scientific), followed by RT-qPCR analysis using SYBR Green Master mix (Bio-Rad) and the iQ5 Multicolour Real-Time PCR Detection System (Bio-Rad). Target genes were amplified using specific primers (Table S3). The ΔΔCt method was applied to calculate the levels of gene expression, relative to a control condition.

DNA sequencing of ZEB1 KO clones

To verify KO on a genomic level, DNA was isolated using the Purelink gDNA mini kit (Thermo Fisher Scientific). The region flanking the gRNA targeting *ZEB1* was amplified using Taq DNA polymerase (Thermo Fisher Scientific) with primers as indicated in Table S3. PCR products were separated using a 1.5% agarose gel, and DNA of specific bands was extracted using the Bioke Gel and PCR cleanup kit (Macherey-Nagel). Cloning of purified PCR products was performed using the InsTA PCR cloning kit (Thermo Fisher Scientific) and subsequently transformed in DH5α cells. For each PCR band identified in the agarose gel electrophoresis, 10 colonies were picked and grown overnight at 37°C. Finally, plasmids were isolated using the Bioke plasmid cleanup kit (Macherey-Nagel). Samples were Sanger sequenced (Macrogen, Amsterdam, the Netherlands) using the M13 reverse primer (Table S3), after which sequencing results were analyzed using Snapgene version 7.2.1.

Chromatin immunoprecipitation analysis

For chromatin immunoprecipitation assays, hPS1 ZEB1 KO cells, rescued with *ZEB1* cDNA (clone 2D12+ZEB1), were cultured for 48 h. One day prior to fixation of the cells, Protein A dynabeads (Thermo Fisher Scientific) were coated with 4 μg ZEB1 (Proteintech 21544-1-AP, Manchester, UK) or 4 μg rabbit IgG control Ab (PP64, Sigma-Aldrich) overnight in PBS/1% BSA (>98% BSA free, Sigma-Aldrich). Cells were fixed by adding 1% formaldehyde (Pharmacy LUMC) for 10 min, followed by quenching using 1/20 volume 2.5 M glycine. After washing twice with PBS, cells were scraped from the plate and lysed using lysis buffer (50 mM Tris-HCl pH 8, 10 mM EDTA, 1% SDS, and EDTA-free protease inhibitors [Sigma-Aldrich]). Samples were sonicated using the Bioruptor Pico (Diagenode, Seraing, Belgium), followed by centrifugation at 11,000 rpm for 10 min to clear debris. A 5% input sample was saved, whereafter the remaining sample was diluted in dilution buffer (20 mM Tris-HCl pH 8, 2 mM EDTA, 1% Triton X-100, 150 mM NaCl, and protease inhibitors). Antibody-bound beads were washed twice and added to the lysate, which was incubated O/N. The following day, samples were washed 5× in RIPA wash buffer (50 mM HEPES-KOH pH 7, 0.5 M LiCl, 1 mM EDTA, 0.7% DOC, and 1% Igepal) and once in TE buffer. 200 μL lysis buffer was added to the beads, followed by vortexing every 2 min for 15 min at 65°C and incubation at 65°C for 6 h. DNA was purified using the Qiaquick PCR purification kit (QIAGEN) and analyzed by qPCR using primers binding in the *F11R* or E-cadherin promoter region (Table S3).

Western blot

Total cell lysates were generated in Pierce RIPA buffer (Thermo Fisher Scientific), supplemented with complete mini protease inhibitor cocktail (Roche Applied Science, Penzberg, Germany). Samples were cleared from cellular debris by centrifugation (13,000 rpm, 4°C, 5 min). Protein concentrations were measured by the Pierce BCA kit (Thermo Fisher Scientific). Lysates were denatured by adding Laemmli sample buffer containing 20 mM DTT and heating for 3 min at 95°C. Equal amounts of protein were separated by gel electrophoresis on 10% SDS-polyacrylamide gels and transferred onto 0.2 μm nitrocellulose membranes using the Trans-Blot Turbo Transfer System (Bio-Rad). Membranes were blocked in TBS, supplemented with 0.1% Tween 20 (TBST) and 10% milk. Antibodies were diluted in TBST containing 5% milk, except for E-cadherin detection, which was incubated in Immuno Booster (Takara Bio Europe, Saint-Germain-en-Laye, France). Primary antibodies were incubated overnight at 4°C and secondary antibodies for 60 min at room temperature. Blots were washed with TBST.

The following primary antibodies were used: mouse anti-vinculin (Sigma-Aldrich, V9131), rabbit anti-ZEB1 (D80D3, Cell Signaling Technology, Leiden, the Netherlands), mouse anti-reovirus σ3 (4F2, Developmental Studies Hybridoma Bank, developed under the auspices of the NICHD and maintained by the University of Iowa, Department of Biology, Iowa City, IA, USA),[48] rat anti-E-cadherin (DECMA-1, Thermo Fisher Scientific), and rabbit anti-vimentin (D21H3, Cell Signaling Technology). Proteins were visualized using the Odyssey CLx Imaging System (LI-COR Biosciences, Bad Homburg, Germany), and western blots were analyzed and quantified using Image Studio Lite software.

Cell viability assays

To determine cell viability following reovirus infection, WST-1 reagent was employed (Roche, Woerden, the Netherlands). Cells were plated in 96-well plates (5–6 wells per condition) and infected with different MOIs of reovirus the following day. After 2–6 days, 20× diluted WST-1 reagent in infection medium was added to the wells. Absorption at OD450 was measured using a plate reader (ENZ-INS-A96, Enzo Life Sciences, Brussels, Belgium), and the percentages of cell viability were calculated by dividing the OD450 values of the virus-treated wells by the values of the mock condition.

Caspase assays

To detect caspase 3/7 activation following reovirus infection, the CellEvent caspase-3/7 green detection reagent (Thermo Fisher Scientific) was used. Cells were plated in triplicate in 96-well plates and infected with reovirus R124 at MOI 10 the following day.

Phase-contrast images, GFP images, and quantifications of the GFP signal (excitation 500 nm, emission 530 nm) were taken every 30 min for a maximum of 48 h using a Cytation microplate reader (Biotek). Images were analyzed using Fiji version 2.14.0.

Statistical analysis

Data are presented as means ± standard deviation from representative experiments of independent replicates. Differences between more than 2 groups were measured using one-way analysis of variance (ANOVA) or two-way ANOVA, depending on the number of variables, and corrected for multiple testing. All analyses were performed using GraphPad Prism version 10.2.3 (San Diego, CA, USA). p values of 0.05 or less were considered statistically significant.

DATA AND CODE AVAILABILITY

Raw sequencing data can be accessed on Gene Expression Omnibus (GEO) under accession number GSE290358. The processed list of genes found from the CRISPR-Cas9 screen can be found in Tables S4 and S5. All other data are included in the manuscript or supplemental data.

ACKNOWLEDGMENTS

Part of this work was carried out at the CRISPR Functional Genomics facility (CFG) at Karolinska Institutet funded by Science for Life Laboratory. C.F.G. acknowledges support from the Swedish National Genomics Infrastructure, the National Academic Infrastructure for Supercomputing in Sweden (NAISS), and the Uppsala Multidisciplinary Center for Advanced Computational Science (UPPMAX). We further thank H. Kocher for providing us with the hPS1 cell line. The graphical abstract and Figure 1A were created using Biorender.com. N.D. is sponsored by funding from the foundation "Overleven met Alvleesklierkanker" (Leiden, the Netherlands) (SOAK 21.02), obtained by V.K. T.J.H. is sponsored by a personal MD-PhD grant from the Leiden University Medical Center and received personal funding from the Dutch Society for Medical Oncology (Utrecht, the Netherlands) to perform the genome-wide CRISPR-Cas9 KO screen at the Karolinska Institutet. V.K. is supported by a personal grant from the Dutch Research Council (NWO-talent program Veni, ZonMw).

AUTHOR CONTRIBUTIONS

N.D. and T.J.H. planned and performed the majority of the experiments and performed data analysis. T.J.H. and B.S. performed the CRISPR-Cas9 KO screen. H.D. performed analysis of the CRISPR-Cas9 KO screen. G.I. performed DNA sequencing of the ZEB1 KO clones. V.K. and L.J.A.C.H. supervised the project. N.D., T.J.H., L.J.A.C.H., and V.K. co-wrote the manuscript. All authors contributed to critically reviewing the manuscript.

DECLARATION OF INTERESTS

The authors declare no competing interests.

SUPPLEMENTAL INFORMATION

Supplemental information can be found online at https://doi.org/10.1016/j.omton.2025.201071.

REFERENCES

1. Macedo, N., Miller, D.M., Haq, R., and Kaufman, H.L. (2020). Clinical landscape of oncolytic virus research in 2020. J. Immunother. Cancer *8*, e001486.
2. Yokoda, R., Nagalo, B.M., Arora, M., Egan, J.B., Bogenberger, J.M., DeLeon, T.T., Zhou, Y., Ahn, D.H., and Borad, M.J. (2017). Oncolytic virotherapy in upper gastrointestinal tract cancers. Oncolytic Virother. *7*, 13–24.
3. Kaufman, H.L., Kohlhapp, F.J., and Zloza, A. (2015). Oncolytic viruses: a new class of immunotherapy drugs. Nat. Rev. Drug Discov. *14*, 642–662.
4. Jhawar, S.R., Thandoni, A., Bommareddy, P.K., Hassan, S., Kohlhapp, F.J., Goyal, S., Schenkel, J.M., Silk, A.W., and Zloza, A. (2017). Oncolytic Viruses-Natural and Genetically Engineered Cancer Immunotherapies. Front. Oncol. *7*, 202.
5. Gascard, P., and Tlsty, T.D. (2016). Carcinoma-associated fibroblasts: orchestrating the composition of malignancy. Genes Dev. *30*, 1002–1019.
6. Everts, A., Bergeman, M., McFadden, G., and Kemp, V. (2020). Simultaneous Tumor and Stroma Targeting by Oncolytic Viruses. Biomedicines *8*, 474.
7. Sahai, E., Astsaturov, I., Cukierman, E., DeNardo, D.G., Egeblad, M., Evans, R.M., Fearon, D., Greten, F.R., Hingorani, S.R., Hunter, T., et al. (2020). A framework for advancing our understanding of cancer-associated fibroblasts. Nat. Rev. Cancer *20*, 174–186.
8. Valkenburg, K.C., de Groot, A.E., and Pienta, K.J. (2018). Targeting the tumour stroma to improve cancer therapy. Nat. Rev. Clin. Oncol. *15*, 366–381.
9. Seager, R.J., Hajal, C., Spill, F., Kamm, R.D., and Zaman, M.H. (2017). Dynamic interplay between tumour, stroma and immune system can drive or prevent tumour progression. Converg. Sci. Phys. Oncol. *3*, 034002.
10. Öhlund, D., Handly-Santana, A., Biffi, G., Elyada, E., Almeida, A.S., Ponz-Sarvise, M., Corbo, V., Oni, T.E., Hearn, S.A., Lee, E.J., et al. (2017). Distinct populations of inflammatory fibroblasts and myofibroblasts in pancreatic cancer. J. Exp. Med. *214*, 579–596.
11. Hartmann, K.P., van Gogh, M., Freitag, P.C., Kast, F., Nagy-Davidescu, G., Borsig, L., and Plückthun, A. (2023). FAP-retargeted Ad5 enables in vivo gene delivery to stromal cells in the tumor microenvironment. Mol. Ther. *31*, 2914–2928.
12. Jing, Y., Chavez, V., Ban, Y., Acquavella, N., El-Ashry, D., Pronin, A., Chen, X., and Merchan, J.R. (2017). Molecular Effects of Stromal-Selective Targeting by uPAR-Retargeted Oncolytic Virus in Breast Cancer. Mol. Cancer Res. *15*, 1410–1420.
13. Huang, T., Wang, H., Chen, N.G., Frentzen, A., Minev, B., and Szalay, A.A. (2015). Expression of anti-VEGF antibody together with anti-EGFR or anti-FAP enhances tumor regression as a result of vaccinia virotherapy. Mol. Ther. Oncolytics *2*, 15003.
14. Harryvan, T.J., Golo, M., Dam, N., Schoonderwoerd, M.J.A., Farshadi, E.A., Hornsveld, M., Hoeben, R.C., Hawinkels, L.J.A.C., and Kemp, V. (2022). Gastrointestinal cancer-associated fibroblasts expressing Junctional Adhesion Molecule-A are amenable to infection by oncolytic reovirus. Cancer Gene Ther. *29*, 1918–1929.
15. Ilkow, C.S., Marguerie, M., Batenchuk, C., Mayer, J., Ben Neriah, D., Cousineau, S., Falls, T., Jennings, V.A., Boileau, M., Bellamy, D., et al. (2015). Reciprocal cellular cross-talk within the tumor microenvironment promotes oncolytic virus activity. Nat. Med. *21*, 530–536.
16. Bots, S.T.F., Harryvan, T.J., Groeneveldt, C., Kinderman, P., Kemp, V., van Montfoort, N., and Hoeben, R.C. (2024). Preclinical evaluation of the gorilla-derived HAdV-B AdV-lumc007 oncolytic adenovirus 'GoraVir' for the treatment of pancreatic ductal adenocarcinoma. Mol. Oncol. *18*, 1245–1258.
17. Kurisu, N., Kaminade, T., Eguchi, M., Ishigami, I., Mizuguchi, H., and Sakurai, F. (2021). Oncolytic reovirus-mediated killing of mouse cancer-associated fibroblasts. Int. J. Pharm. *610*, 121269.
18. Zhang, P., Sun, Y., and Ma, L. (2015). ZEB1: at the crossroads of epithelial-mesenchymal transition, metastasis and therapy resistance. Cell Cycle *14*, 481–487.
19. Hartmann, C., Schwietzer, Y.A., Otani, T., Furuse, M., and Ebnet, K. (2020). Physiological functions of junctional adhesion molecules (JAMs) in tight junctions. Biochim. Biophys. Acta. Biomembr. *1862*, 183299.
20. Doench, J.G., Fusi, N., Sullender, M., Hegde, M., Vaimberg, E.W., Donovan, K.F., Smith, I., Tothova, Z., Wilen, C., Orchard, R., et al. (2016). Optimized sgRNA design to maximize activity and minimize off-target effects of CRISPR-Cas9. Nat. Biotechnol. *34*, 184–191.
21. Jongsma, M.L.M., de Waard, A.A., Raaben, M., Zhang, T., Cabukusta, B., Platzer, R., Blomen, V.A., Xagara, A., Verkerk, T., Bliss, S., et al. (2021). The SPPL3-Defined Glycosphingolipid Repertoire Orchestrates HLA Class I-Mediated Immune Responses. Immunity *54*, 132–150.e9.
22. Stirnemann, J., Belmatoug, N., Camou, F., Serratrice, C., Froissart, R., Caillaud, C., Levade, T., Astudillo, L., Serratrice, J., Brassier, A., et al. (2017). A Review of Gaucher Disease Pathophysiology, Clinical Presentation and Treatments. Int. J. Mol. Sci. *18*, 441.

23. Jesnowski, R., Fürst, D., Ringel, J., Chen, Y., Schrödel, A., Kleeff, J., Kolb, A., Schareck, W.D., and Löhr, M. (2005). Immortalization of pancreatic stellate cells as an in vitro model of pancreatic fibrosis: deactivation is induced by matrigel and N-acetylcysteine. Lab. Invest. *85*, 1276–1291.

24. Froeling, F.E.M., Mirza, T.A., Feakins, R.M., Seedhar, A., Elia, G., Hart, I.R., and Kocher, H.M. (2009). Organotypic culture model of pancreatic cancer demonstrates that stromal cells modulate E-cadherin, beta-catenin, and Ezrin expression in tumor cells. Am. J. Pathol. *175*, 636–648.

25. Schoonderwoerd, M.J.A., Hakuno, S.K., Sassen, M., Kuhlemaijer, E.B., Paauwe, M., Slingerland, M., Fransen, M.F., and Hawinkels, L.J.A.C. (2021). Targeting Endoglin Expressing Cells in the Tumor Microenvironment Does Not Inhibit Tumor Growth in a Pancreatic Cancer Mouse Model. OncoTargets Ther. *14*, 5205–5220.

26. Ungewiss, C., Rizvi, Z.H., Roybal, J.D., Peng, D.H., Gold, K.A., Shin, D.H., Creighton, C.J., and Gibbons, D.L. (2016). The microRNA-200/Zeb1 axis regulates ECM-dependent β1-integrin/FAK signaling, cancer cell invasion and metastasis through CRKL. Sci. Rep. *6*, 18652.

27. Maginnis, M.S., Forrest, J.C., Kopecky-Bromberg, S.A., Dickeson, S.K., Santoro, S.A., Zutter, M.M., Nemerow, G.R., Bergelson, J.M., and Dermody, T.S. (2006). β1 Integrin Mediates Internalization of Mammalian Reovirus. J. Virol. *80*, 2760–2770.

28. Perez-Oquendo, M., and Gibbons, D.L. (2022). Regulation of ZEB1 Function and Molecular Associations in Tumor Progression and Metastasis. Cancers (Basel) *14*, 1864.

29. Eger, A., Aigner, K., Sonderegger, S., Dampier, B., Oehler, S., Schreiber, M., Berx, G., Cano, A., Beug, H., and Foisner, R. (2005). DeltaEF1 is a transcriptional repressor of E-cadherin and regulates epithelial plasticity in breast cancer cells. Oncogene *24*, 2375–2385.

30. Howells, A., Marelli, G., Lemoine, N.R., and Wang, Y. (2017). Oncolytic Viruses-Interaction of Virus and Tumor Cells in the Battle to Eliminate Cancer. Front. Oncol. *7*, 195.

31. Rosen, L., Evans, H.E., and Spickard, A. (1963). Reovirus infections in human volunteers. Am. J. Hyg. *77*, 29–37.

32. Tang, B., Guo, Z.S., Bartlett, D.L., Liu, J., McFadden, G., Shisler, J.L., and Roy, E.J. (2019). A cautionary note on the selectivity of oncolytic poxviruses. Oncolytic Virother. *8*, 3–8.

33. van den Wollenberg, D.J.M., Dautzenberg, I.J.C., van den Hengel, S.K., Cramer, S.J., de Groot, R.J., and Hoeben, R.C. (2012). Isolation of Reovirus T3D Mutants Capable of Infecting Human Tumor Cells Independent of Junction Adhesion Molecule-A. PLoS One *7*, e48064.

34. Sanchez-Tillo, E., Lazaro, A., Torrent, R., Cuatrecasas, M., Vaquero, E.C., Castells, A., Engel, P., and Postigo, A. (2010). ZEB1 represses E-cadherin and induces an EMT by recruiting the SWI/SNF chromatin-remodeling protein BRG1. Oncogene *29*, 3490–3500.

35. Schmalhofer, O., Brabletz, S., and Brabletz, T. (2009). E-cadherin, beta-catenin, and ZEB1 in malignant progression of cancer. Cancer Metastasis Rev. *28*, 151–166.

36. Fong, D., Spizzo, G., Mitterer, M., Seeber, A., Steurer, M., Gastl, G., Brosch, I., and Moser, P. (2012). Low expression of junctional adhesion molecule A is associated with metastasis and poor survival in pancreatic cancer. Ann. Surg Oncol. *19*, 4330–4336.

37. Sakata, J., Utsumi, F., Suzuki, S., Niimi, K., Yamamoto, E., Shibata, K., Senga, T., Kikkawa, F., and Kajiyama, H. (2017). Inhibition of ZEB1 leads to inversion of metastatic characteristics and restoration of paclitaxel sensitivity of chronic chemoresistant ovarian carcinoma cells. Oncotarget *8*, 99482–99494.

38. Menche, C., Schuhwerk, H., Armstark, I., Gupta, P., Fuchs, K., van Roey, R., Mosa, M.H., Hartebrodt, A., Hajjaj, Y., Clavel Ezquerra, A., et al. (2024). ZEB1-mediated fibroblast polarization controls inflammation and sensitivity to immunotherapy in colorectal cancer. EMBO Rep. *25*, 3406–3431.

39. Fu, R., Han, C.-F., Ni, T., Di, L., Liu, L.-J., Lv, W.-C., Bi, Y.-R., Jiang, N., He, Y., Li, H.-M., et al. (2019). A ZEB1/p53 signaling axis in stromal fibroblasts promotes mammary epithelial tumours. Nat. Commun. *10*, 3210.

40. Wang, J., Lee, S., Teh, C.E.Y., Bunting, K., Ma, L., and Shannon, M.F. (2009). The transcription repressor, ZEB1, cooperates with CtBP2 and HDAC1 to suppress IL-2 gene activation in T cells. Int. Immunol. *21*, 227–235.

41. Ebnet, K. (2017). Junctional Adhesion Molecules (JAMs): Cell Adhesion Receptors With Pleiotropic Functions in Cell Physiology and Development. Physiol. Rev. *97*, 1529–1554.

42. Wang, J., and Chen, X. (2022). Junctional Adhesion Molecules: Potential Proteins in Atherosclerosis. Front. Cardiovasc. Med. *9*, 888818.

43. Hou, Y., Rabquer, B.J., Gerber, M.L., Del Galdo, F., Jimenez, S.A., Haines, G.K., Barr, W.G., Massa, M.C., Seibold, J.R., and Koch, A.E. (2010). Junctional adhesion molecule-A is abnormally expressed in diffuse cutaneous systemic sclerosis skin and mediates myeloid cell adhesion. Ann. Rheum. Dis. *69*, 249–254.

44. Cross, B.C.S., Lawo, S., Archer, C.R., Hunt, J.R., Yarker, J.L., Riccombeni, A., Little, A.S., McCarthy, N.J., and Moore, J.D. (2016). Increasing the performance of pooled CRISPR-Cas9 drop-out screening. Sci. Rep. *6*, 31782.

45. Schmierer, B., Botla, S.K., Zhang, J., Turunen, M., Kivioja, T., and Taipale, J. (2017). CRISPR/Cas9 screening using unique molecular identifiers. Mol. Syst. Biol. *13*, 945.

46. Li, W., Xu, H., Xiao, T., Cong, L., Love, M.I., Zhang, F., Irizarry, R.A., Liu, J.S., Brown, M., and Liu, X.S. (2014). MAGeCK enables robust identification of essential genes from genome-scale CRISPR/Cas9 knockout screens. Genome Biol. *15*, 554.

47. Dull, T., Zufferey, R., Kelly, M., Mandel, R.J., Nguyen, M., Trono, D., and Naldini, L. (1998). A third-generation lentivirus vector with a conditional packaging system. J. Virol. *72*, 8463–8471.

48. Virgin, H.W., Mann, M.A., Fields, B.N., and Tyler, K.L. (1991). Monoclonal antibodies to reovirus reveal structure/function relationships between capsid proteins and genetics of susceptibility to antibody action. J. Virol. *65*, 6772–6781.